

SUPPRESSION OF MICROBUNCHING INSTABILITY THROUGH DISPERSIVE LATTICE

Biaobin Li^{1,2}, Ji Qiang^{2,*}

¹ University of Science and Technology of China, 230029, Hefei, China

² Lawrence Berkeley National Laboratory, 94720, Berkeley, USA

Abstract

The microbunching instability from the initial small modulation such as shot-noise can be amplified by longitudinal space-charge force and causes significant electron beam quality degradation at the exit of accelerator for the next generation x-ray free electron laser. In the paper, we present analytical and numerical simulation studies of a novel method using dispersion leakage from a quadrupole inside a bunch compressor chicane.

INTRODUCTION

The microbunching instability in linacs can limit the performance of single-pass x-ray FELs by significantly degrading the electron beam quality [1–5]. The conventional method to control the instability is to use a laser heater to increase the beam uncorrelated energy spread before bunch compressors [2, 6], which is typically tolerable for operation of self-amplified spontaneous emission (SASE) FELs. However, for seeded FELs it could limit the FEL gain [7]. Recently alternative techniques [8–13] based on transverse-to-longitudinal coupling terms (R_{51}, R_{52}) or (R_{53}, R_{54}) are proposed to suppress the microbunching instability. These schemes are quite attractive because of the "reversible feature", which means the transverse emittance and slice energy spread can be recovered meanwhile effectively suppressing the microbunching instability [14]. Among these methods, the scheme based on two bending magnets [9] is quite simple without expensive hardware, however the use of bending magnets will change the beam line direction, which is not convenient and difficult to apply to the existing FEL facilities.

In this paper, we propose a simple scheme to suppress the microbunching instability by inserting a quadrupole into a four dipoles bunch compressor to introduce the longitudinal mixing terms to suppress the instability. Theoretical analysis and numerical simulations including longitudinal and transverse space charge are given to show the feasibility of this scheme.

METHODS

We consider the machine layout shown in Fig. 1. One quadrupole is placed in the middle of BC1 to leak out the longitudinal mixing terms R_{51} and R_{52} for instability suppression. The energy chirp induced in Linac-2 is canceled out in Linac-3. For the energy chirp generated in Linac-1, it

is maintained after Linac-3, which calls for an isochronous dogleg design to avoid further bunch length compression.

The longitudinal phase space smearing brought up by the coupling terms in BC1 can significantly smooth the upstream density and energy modulation, thus suppresses further instability amplifications in the following section of the accelerator. Meanwhile, due to the existence of energy chirp right before BC1, additional slice energy spread will also be introduced by the coupling terms, which can effectively suppress the possible growth of the intrinsic and residual shot-noise modulation between the BC1 and the dogleg. Following the equations in [12, 15], the slice energy spread after the BC1 is given as:

$$\sigma_\delta(s_3) \approx C_1 h_1 R_{51}^A \sigma_x(s_2), \quad (1)$$

where C_1 is the compression factor from s_1 to s_3 , h_1 and $\sigma_x(s_2)$ are the energy chirp and the horizontal rms beam size before the BC1, R_{51}^A is the coupling term from the BC1 section. Finally, the extra slice energy spread and the transverse emittance can be restored by adjusting the quadrupoles inside the dogleg, which cancels the induced couplings and makes the whole system an achromat.

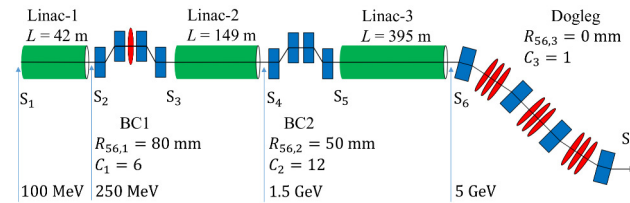


Figure 1: (color online). Scheme Layout.

Here the linear transfer matrices R ($R = R^B T, R^A$) from s_2 to s_7 in (x, x', z, δ) coordinates are given in the above scheme, where R^A is the transfer matrix of $s_2 \rightarrow s_3$,

$$R^A = \begin{pmatrix} R_{11}^A & R_{12}^A & 0 & R_{16}^A \\ R_{21}^A & R_{22}^A & 0 & R_{26}^A \\ R_{51}^A & R_{52}^A & 1 & R_{56,1}^A \\ 0 & 0 & 0 & 1 \end{pmatrix}, \quad (2)$$

R^B is the transfer matrix through the dogleg section $s_6 \rightarrow s_7$,

$$R^B = \begin{pmatrix} R_{11}^B & R_{12}^B & 0 & R_{16}^B \\ R_{21}^B & R_{22}^B & 0 & R_{26}^B \\ R_{51}^B & R_{52}^B & 1 & 0 \\ 0 & 0 & 0 & 1 \end{pmatrix}, \quad (3)$$

This is a preprint — the final version is published with IOP

Content from this work may be used under the terms of the CC BY 3.0 licence (© 2019). Any distribution of this work must maintain attribution to the author(s), title of the work, publisher, and DOI

* jqiang@lbl.gov

Content from this work may be used under the terms of the CC BY 3.0 licence (© 2019). Any distribution of this work must maintain attribution to the author(s), title of the work, publisher, and DOI

T_r is the middle accelerator section from $s_3 \rightarrow s_6$

$$T_r = \begin{pmatrix} r_{11} & r_{12} & 0 & 0 \\ r_{21} & r_{22} & 0 & 0 \\ 0 & 0 & (1 + \zeta)/C_2 & R_{56,2}E_3/E_5 \\ 0 & 0 & 0 & (C_2E_3/E_7)/(1 + \zeta) \end{pmatrix}, \quad (4)$$

where $\zeta = (C_1 - 1)C_2(R_{56,2}E_3)/(R_{56,1}E_5)$, E_j is the beam energy at position s_j . By using the symplectic condition of the transfer matrices ($R^T \cdot S \cdot R = S \cdot E_{final}/E_{initial}$) when taking acceleration effects into account and designing the dogleg section so that

$$R_{51}^B = \frac{[r_{21}(R_{52}^A R_{11}^A - R_{51}^A R_{12}^A) + r_{22}(R_{52}^A R_{21}^A - R_{51}^A R_{22}^A)]}{C_2/(1 + \zeta E_7/E_3)},$$

$$R_{52}^B = \frac{[-r_{11}(R_{52}^A R_{11}^A - R_{51}^A R_{12}^A) - r_{12}(R_{52}^A R_{21}^A - R_{51}^A R_{22}^A)]}{C_2/[(1 + \zeta)E_7/E_3]}, \quad (5)$$

the entire transport system can be made an achromat with the linear transfer matrix from s_2 to s_7

$$R_{s_2 \rightarrow s_7} = \begin{pmatrix} R_{11} & R_{12} & 0 & 0 \\ R_{21} & R_{22} & 0 & 0 \\ 0 & 0 & (1 + \zeta)/C_2 & \frac{R_{56,1} + C_1 R_{56,2} E_3}{C_2} \\ 0 & 0 & 0 & \frac{C_2 E_3}{(1 + \zeta) E_7} \end{pmatrix}. \quad (6)$$

OPTICS DESIGN

The optics design based on the first-order transfer map without collective effects are given in this section. The normalized quadrupole strength (K_1) in BC1 is 0.83/m² with 0.2 m length in this example. This leaks out $R_{51}^A = 0.05$, $R_{52}^A = 0.18$ m for microbunching instability suppression. Generally, a stronger quadrupole in the BC1 will generate stronger instability suppression. However, the dispersion leakage and beam tilt after the BC1 will make the beam size in horizontal direction more difficult to control. The maximum rms beam size after the BC1 is about 3 mm in this example with the initial beam bunch length of 3 mm as shown in the left plot of Fig. 2. The initial beam transverse distribution is a uniform round cross section with 0.4 mm radius and 0.3 mm·mrad normalized transverse emittance with a flattop current of 20 A. The initial uncorrelated energy spread is 2 keV with zero energy chirp. The beam is accelerated from 100 MeV to finally 5 GeV with a total compression factor of 72. The beam transverse size at the entrance of BC1 is matched back to the initial beam radius 0.4 mm. Evolution of the transverse normalized emittance is shown in the right plot of Fig. 2, horizontal emittance is restored after tuning the quadrupoles in the dogleg section according to Eq. (5) with the help of optimization tools of the Elegant [16].

THEORETICAL ANALYSIS

As the whole section $s_2 \rightarrow s_7$ is an achromat but with non-zero R_{56} , the energy or density modulation induced

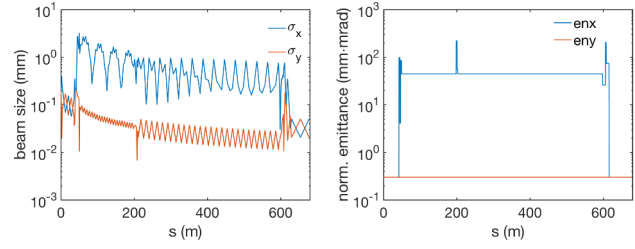


Figure 2: (color online). Evolution of the beam transverse rms radius (left plot) and normalized transverse emittance (right plot) along the longitudinal position.

before the BC1 will still be amplified after electron beam passing through the dogleg because of the reversible feature. By leaking some dispersion out from the reversible system, this part of amplification may also be suppressed [12]. We here focus on the instability suppression in $s_2 \rightarrow s_7$ section, neglecting the collective effects in Linac-1. Solving the microbunching integral equation provided in [17, 18] and following the equations in [9], as the $R_{56}(s_{5 \rightarrow 7})$ is zero, which drops off the amplification term due to the energy modulation induced by collective effects inside Linac-3 and also the coupled collective effects amplification term between Linac-2 and Linac-3, finally only two terms are left in Eq. (7). Assuming an electron beam with zero energy chirp and an initial current modulation factor b_0 at the entrance to Linac-1, the final density modulation factor is given as

$$b[k(s_7); s_7] = b_1[k(s_7); s_7] + b_2[k(s_7); s_7], \quad (7)$$

where $k(s) = C(s)k_0$, $C(s)$ is the compression factor and k_0 is the initial modulation wavenumber. Here $b_1[k(s_7); s_7]$ describes the evolution of modulation factor in the absence of all collective effects, and is given as

$$b_1[k(s_7); s_7] = b_0 \exp[-k^2(s_7) \hat{R}_{56}^2(s_{1 \rightarrow 7}) \sigma_{\delta_0}^2 / 2]; \quad (8)$$

the second term b_2 describes the amplification due to collective effects between Linac-2 section, and is given as

$$b_2[k(s_7); s_7] = ib_0 k(s_7) \hat{R}_{56}(s_{3 \rightarrow 7}) \frac{I(s_3)}{\gamma_0} \hat{Z}(s_{3 \rightarrow 4})$$

$$\times \exp\left(\frac{-k_0^2 \mathcal{D}^2(s_{3 \rightarrow 7}) \sigma_{\delta_0}^2}{2}\right)$$

$$\times \exp\left(\frac{-k_0^2 \mathcal{H}(s_{3 \rightarrow 7}) \epsilon_{x,n}}{2\gamma_0 \beta_{x0}}\right). \quad (9)$$

The impedance term above is defined as

$$\hat{Z}(s_{j \rightarrow k}) = \int_{s_j}^{s_k} \frac{4\pi Z[k(\tau); \tau]}{I_A Z_0} d\tau,$$

where $Z[k(\tau); \tau]$ is the impedance per unit length of collective effects and Z_0 is the vacuum impedance, I_A is the Alfvén current, σ_{δ_0} is the initial rms relative energy spread, γ_0 is the initial electron beam relativistic factor, $\epsilon_{x,n}$ is the normalized horizontal emittance, $I(s_j) = C(s_j)I_0$, I_0 is the

initial current. The exponential damping to the modulation amplification due to initial energy spread and transverse-to-longitudinal coupling is given by:

$$\begin{aligned} \mathcal{D}^2(s_{3 \rightarrow 7}) &= U^2(s_7, s_3) + U^2(s_3, s_1), \\ \mathcal{H}(s_{3 \rightarrow 7}) &= T(s_7, s_3) + T(s_3, s_1), \end{aligned} \quad (10)$$

where $T(s, \tau) = (\beta_{x0}V - \alpha_{x0}W)^2 + W^2$, and

$$\begin{aligned} U(s, \tau) &= C(s)\hat{R}_{56}(s) - C(\tau)\hat{R}_{56}(\tau), \\ V(s, \tau) &= C(s)\hat{R}_{51}(s) - C(\tau)\hat{R}_{51}(\tau), \\ W(s, \tau) &= C(s)\hat{R}_{52}(s) - C(\tau)\hat{R}_{52}(\tau), \end{aligned} \quad (11)$$

where β_{x0} and α_{x0} are the initial horizontal Twiss parameters. Here, we used the shorthand notation $\hat{R}_{mn}(s) = \hat{R}_{mn}(s_1 \rightarrow s)$, where \hat{R}_{mn} is defined as $\hat{R}_{mn}(s_{j \rightarrow k}) = R_{mn}(s_{j \rightarrow k})\gamma_0/\gamma_j$, in order to include acceleration effects [4].

SIMULATION

To verify the above scheme, we simulated an electron beam with an initial 0.6% current modulation at $140 \mu\text{m}$ wavelength and the initial beam parameters described in the optics design section, transporting through the accelerator system shown in Fig. 1 with the quadrupole in BC1 turned off and on using IMPACT [19]. We modified the source code to transport particles using first-order transfer map, but taking into account both the longitudinal space charge (LSC) and the transverse space charge (TSC) effects, to benchmark our analytical calculations.

Figures 3 and 4 show the final longitudinal phase space distributions, the projected current, the final horizontal normalized slice emittance, and the slice energy spread at the exit of dogleg with residual energy chirp removed manually. With the help of the coupling terms leaking out from BC1, both energy and current modulations are greatly suppressed. The slice energy spread after BC1 is enlarged to about 156 keV in the simulation, which agrees well with Eq. (1). The additional slice energy spread greatly suppressed the instability amplification process in $s_{3 \rightarrow 6}$ section, which showed smooth density profile from the simulation. The final rms uncorrelated energy spread of the core beam section is restored back to about 150 keV, slightly larger than 144 keV which is the value of the initial uncorrelated energy spread enlarged by the total compression factor. The slice emittance in the core beam section shows about 60% growth when LSC and TSC are taken into account.

Figure 5 shows the total gain after dogleg with quadrupole in BC1 turned off and on based on the linear theory along with IMPACT simulation results. The analytical gain and the simulation results agree quite well. The slight discrepancies in short wavelength could be due to the approximation involved in the space-charge impedance model used in the linear theory.

CONCLUSIONS

In this paper, a simple microbunching instability suppression scheme using a quadrupole inserting into a buncher

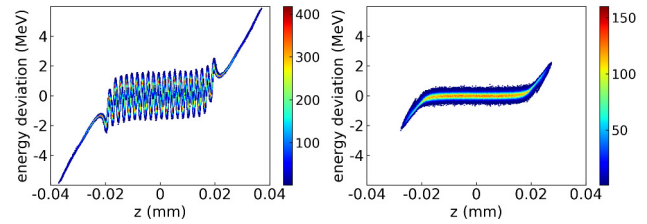


Figure 3: (color online). Final longitudinal phase space when quadrupole in BC1 is turned off (left plot) and on (right plot).

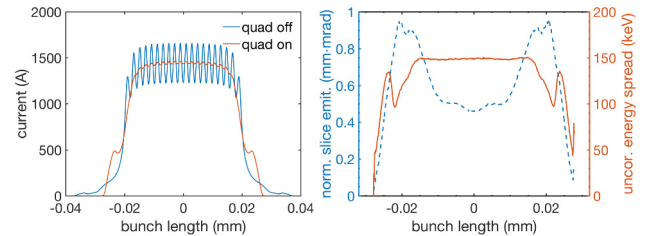


Figure 4: (color online). Left plot, Final projected current when quadrupole in BC1 is turned off and on. Right plot, final horizontal normalized slice emittance (dashed line) and slice energy spread (solid line) with the quadrupole in BC1 turned on.

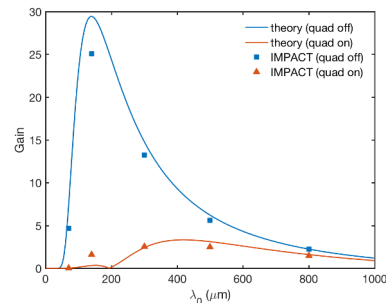


Figure 5: (color online). Microbunching gain defined as $|b[k(s_7); s_7]/b_0|$ when quadrupole in BC1 is turned off and on.

compressor BC1 is proposed. The increased slice energy spread and the horizontal-to-longitudinal smearing after the BC1 are efficiently applied to suppress the density and energy modulations in this scheme. The final slice energy spread is almost restored back to the nominal energy spread after the dogleg section. The factor that causes the final slice emittance growth is still under study. More detailed work including coherent synchrotron radiation (CSR), the accelerator transverse structure wakefield effects, and the nonlinear transfer map will be carried out in our future work.

ACKNOWLEDGMENTS

This work was supported by the U.S. Department of Energy under Contract No. DE-AC02-05CH11231. One of the authors, B. L., thanks China Scholarship Council for financial support (CSC File No. 201706340072).

REFERENCES

- [1] M Borland, YC Chae, P Emma, JW Lewellen, V Bharadwaj, WM Fawley, P Krejcik, C Limborg, SV Milton, and H-D Nuhn. Start-to-end simulation of self-amplified spontaneous emission free electron lasers from the gun through the undulator. *Nuclear Instruments and Methods in Physics Research Section A: Accelerators, Spectrometers, Detectors and Associated Equipment*, 483(1-2):268–272, 2002.
- [2] EL Saldin, EA Schneidmiller, and MV Yurkov. Longitudinal space charge-driven microbunching instability in the tesla test facility linac. *Nuclear Instruments and Methods in Physics Research. Section A, Accelerators, Spectrometers, Detectors and Associated Equipment*, 528(1-2):355–359, 2004.
- [3] Zhirong Huang, M Borland, P Emma, J Wu, C Limborg, G Stupakov, and J Welch. Suppression of microbunching instability in the linac coherent light source. *Physical Review Special Topics-Accelerators and Beams*, 7(7):074401, 2004.
- [4] Marco Venturini. Microbunching instability in single-pass systems using a direct two-dimensional vlasov solver. *Physical Review Special Topics-Accelerators and Beams*, 10(10):104401, 2007.
- [5] RA Bosch, KJ Kleman, and J Wu. Modeling two-stage bunch compression with wakefields: Macroscopic properties and microbunching instability. *Physical Review Special Topics-Accelerators and Beams*, 11(9):090702, 2008.
- [6] Zhirong Huang, A Brachmann, F-J Decker, Y Ding, D Dowell, P Emma, J Frisch, S Gilevich, G Hays, and Ph Hering. Measurements of the linac coherent light source laser heater and its impact on the x-ray free-electron laser performance. *Physical Review Special Topics-Accelerators and Beams*, 13(2):020703, 2010.
- [7] Li Hua Yu. Generation of intense uv radiation by subharmonically seeded single-pass free-electron lasers. *Physical Review A*, 44(8):5178, 1991.
- [8] Christopher Behrens, Zhirong Huang, and Dao Xiang. Reversible electron beam heating for suppression of microbunching instabilities at free-electron lasers. *Physical Review Special Topics-Accelerators and Beams*, 15(2):022802, 2012.
- [9] Ji Qiang, Chad E Mitchell, and Marco Venturini. Suppression of microbunching instability using bending magnets in free-electron-laser linacs. *Physical review letters*, 111(5):054801, 2013.
- [10] Chao Feng, Dazhang Huang, Haixiao Deng, Qiang Gu, and Zhentang Zhao. Suppression of microbunching instability via a transverse gradient undulator. *New Journal of Physics*, 17(7):073028, 2015.
- [11] Dazhang Huang, Chao Feng, Haixiao Deng, Qiang Gu, and Zhentang Zhao. Transverse to longitudinal phase space coupling in an electron beam for suppression of microbunching instability. *Physical Review Accelerators and Beams*, 19(10):100701, 2016.
- [12] Tao Liu, Weilun Qin, Dong Wang, and Zhirong Huang. Reversible beam heater for suppression of microbunching instability by transverse gradient undulators. *Physical Review Accelerators and Beams*, 20(8):082801, 2017.
- [13] Biaobin Li and Ji Qiang. Suppression of Microbunching Instability Using a Quadrupole Inserted Chicane in Free-Electron-Laser Linacs. *Proc. IPAC2018, THPMF082, Vancouver, Canada*, 2018.
- [14] Zhirong Huang and Gennady Stupakov. Control and application of beam microbunching in high brightness linac-driven free electron lasers. *Nuclear Instruments and Methods in Physics Research. Section A, Accelerators, Spectrometers, Detectors and Associated Equipment*, 907(C), 2018.
- [15] Gennady Stupakov and Paul Emma. Reversible electron beam heater without transverse deflecting cavities. *Proceedings of FEL 2015, Daejeon, Korea*, 2015.
- [16] Michael Borland. Elegant: A flexible sdds-compliant code for accelerator simulation. Report, Argonne National Lab., IL (US), 2000.
- [17] Zhirong Huang and Kwang-Je Kim. Formulas for coherent synchrotron radiation microbunching in a bunch compressor chicane. *Physical Review Special Topics-Accelerators and Beams*, 5(7):074401, 2002.
- [18] Stupakov Heifets, G Stupakov, and S Krinsky. Coherent synchrotron radiation instability in a bunch compressor. *Physical Review Special Topics-Accelerators and Beams*, 5(6):064401, 2002.
- [19] Ji Qiang, Robert D Ryne, Salman Habib, and Viktor Decyk. An object-oriented parallel particle-in-cell code for beam dynamics simulation in linear accelerators. *Journal of Computational Physics*, 163(2):434–451, 2000.